Effect of Hydrodynamic Pressure in a 4–Blades Vane Rheometer

Jon E. Wallevik[1]

[1]Innovation Center Iceland, Arleynir 2–8, IS–112 Reykjavik

ABSTRACT

Vane rheometers are often used to obtain rheological flow parameters. In this work, an analysis of the flow phenomenon inside such device is made using the finite volume method utilizing the OpenFOAM 2.1.1. In particular, the shaft torque is calculated at different angular velocities and the effect of hydrodynamic pressure is analyzed separately and compared to the effect generated by viscous stress. The outcome of the overall analysis is that the effect of hydrodynamic pressure constitutes more than 80% of the shaft torque, leaving less than 20% of the torque to viscous stress.

INTRODUCTION

The vane rheometer consists of an impeller rotating in a baffles–cylinder geometry. The one of the objective of this geometrical configuration is to eliminate slip between the sample and the solid boundaries of the rheometer[1,2]. However, with rotation, the impeller's vane blades will both push and drag the fluid, resulting in non–uniform hydrodynamic pressure exerted on the blades. Thus, in addition to the viscous shear stress, this pressure will influence the measured torque registered by the rheometer (i.e. influence the shaft torque). As such, the main question becomes: *How significant is this influence?* Is there a direct relationship between the output of the vane rheometer and the fluid apparent viscosity η, or will the effect of hydrodynamic pressure distort or damage this relationship? Or more to the point, can the results of the vane rheometer be trusted to give an accurate information about the fluid apparent viscosity?

The objective of the current work is to analyze the complex flow phenomenon inside an arbitrary vane rheometer with a special focus on the hydrodynamic pressure and its effect on the shaft torque. With this aim, the CFD software used is the OpenFOAM. It is licensed under the GNU General Public License (GNU GPL) and is available at www.openfoam.org, without charge or annual fee of any kind. The benefits of having a GNU GPL licensed code over a closed commercial code, is that the user has always a full access to the source code, without any restriction, either to understand, correct, modify or enhance the software. OpenFOAM is written in C++. As such, an object–oriented programming approach is used in the creation of data types (fields) that closely mimics those of mathematical field theory[3]. For the code parallelization and communication between processors, the domain decomposition method is used with the Message Passing Interface (MPI)[4].

A modified version of the simpleFoam solver was programmed in this work. The modifications were done so it could handle a so–called single rotating reference frame approach[5] (SRF). In this solver, the three dimensional momentum equation as well as the continuity equation are solved in parallel to obtain the velocity and hydrodynamic pressure profiles throughout

the geometry. More precisely, the pressure velocity coupling is handled with a Semi–Implicit Method for Pressure–Linked Equations (SIMPLE) procedure[6] using a modified Rhie–Chow interpolation for cell centered data storage[7].

MATERIAL MODEL

In this work, the Herschel-Bulkley model is applied (the effect of Newtonian- and Bingham model is well reported elsewhere[1]). With this, the constitutive equation used consists of the Generalized Newtonian Model[8] or in short GNM. The GNM is given by $\mathbf{T} = 2\,\eta\,\dot{\boldsymbol{\varepsilon}}$, where the terms $\mathbf{T}$ and η are the extra stress tensor and the apparent viscosity, respectively[9]. The term $\dot{\boldsymbol{\varepsilon}} = \frac{1}{2}(\nabla\mathbf{U} + (\nabla\mathbf{U})^{\mathrm{T}})$ is known as the rate–of–deformation tensor and $\mathbf{U}$ represents the velocity[10,11].

Oldroyd[12] used a von Mises yield criterion for flow to describe the Bingham fluid. Using such approach (with the above mentioned GNM), the flow behavior of the Herschel-Bulkley model model can be described with

$$\mathbf{T} = 2\,\eta\,\dot{\boldsymbol{\varepsilon}} \quad \text{for} \quad \mathbf{T} : \mathbf{T}/2 \geq \tau_0^2 \tag{1}$$

$$\dot{\boldsymbol{\varepsilon}} = 0 \quad \text{for} \quad \mathbf{T} : \mathbf{T}/2 < \tau_0^2 \tag{2}$$

where the apparent viscosity (or equally, the shear viscosity) is given by

$$\eta = \frac{\tau_0}{\dot{\gamma}} + k\,\dot{\gamma}^{n-1} \tag{3}$$

For incompressible (i.e. $\nabla \cdot \mathbf{U} = 0$) three dimensional flow, where the GNM is valid, it can been shown[1] that $\mathbf{T} : \mathbf{T}/2$ is the shear stress τ, while $\sqrt{2\,\dot{\boldsymbol{\varepsilon}} : \dot{\boldsymbol{\varepsilon}}}$ is the shear rate $\dot{\gamma}$. The term τ_0 is the yield stress [Pa], k is the consistency index [$\mathrm{Pa} \cdot \mathrm{s}^n$], while n is the power-law exponent (unit less).

Because of the nonlinearities in the governing equation and because of the inherent discontinuity in the constitutive equation, a computer simulation of Herschel-Bulkley flow is difficult. As the yield surface is approached, the presence of $\dot{\gamma}$ in the denominator of Eq. (3) makes the extra stress tensor $\mathbf{T}$ unbounded. Furthermore, while simulating the velocity field $\mathbf{U}$, the location of the yield surface is unknown prior to calculation. To overcome these difficulties, a regularized version of the Herschel-Bulkley model Eqs. (1)–(3) is used in this work[1].

EXPERIMENTAL

The vane rheometer used in this work is shown in Fig. 1. Its rotating geometry consists of a shaft (i.e. a rod) connected to four blades. The stationary part consists of a cub that contains the test material.

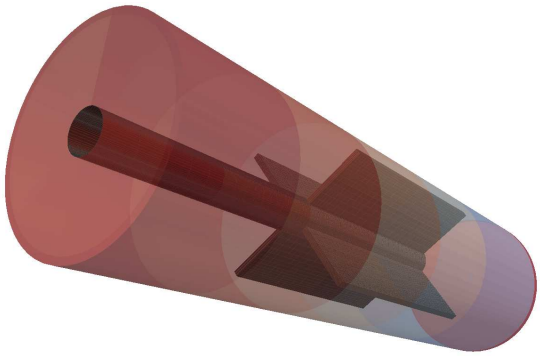

Figure 1. The vane rheometer under consideration.

The thickness of each blade is 1.0 mm. The edge–to–edge diameter of the blades (including the shaft diameter) is 28.0 mm. The diameter of the shaft is 6.0 mm. The diameter of the cub is 30.0 mm. The height of the (rotating) blades is 40.0 mm, while the height of the cub is 110.0 mm. The clearing at the bottom is 30.0 mm.

The number of cells used in generating the vane rheometer is 201,396. The mesh is generated with a native OpenFOAM mesh utility called blockMesh, and the mesh quality is checked with another OpenFOAM utility, named checkMesh. More than 98% of the cells are hexahedra, while the rest consist of prisms.

The no–slip boundary condition (i.e. the Dirichlet boundary condition) is used at all wall boundaries. However, at the top of the rheometer (i.e. at/near the boundary between atmosphere and liquid), the

boundary condition consists of $\mathbf{i}_z \cdot \nabla \mathbf{U} = \partial \mathbf{U}/\partial z = 0$ (i.e. the Neumann boundary condition).

In this work, the yield stress τ_0 is set equal to 0.1 Pa, while the power-law exponent n is equal to 0.5 (i.e. shear thinning fluid) and the density is set equal to $\rho = 990\,\mathrm{kg/m^3}$. The difference between experimental cases rests only in difference in the consistency index k, set equal to 0.1, 1 and 10 $\mathrm{Pa \cdot s^n}$. During a single rheological test, the impeller angular velocity ω range from 0.1 to 0.6 rps (i.e. from 0.6 to 3.8 rad/s), while the cub is stationary.

CALCULATION OF TORQUE

To calculate the shaft torque, the stress acting on the impeller system has to be obtained. This is done by calculating the traction vector[10,11] applied to the shaft and the four blades connected to it, given by $\mathbf{t} = \mathbf{n} \cdot \boldsymbol{\sigma} = \mathbf{n} \cdot (-p\,\mathbf{I} + \mathbf{T})$. The terms $\boldsymbol{\sigma}$, p and $\mathbf{I}$ are the total stress tensor, hydrodynamic pressure and the unit dyadic, respectevly[10,11].

Here, the traction vector is split into two components, namely one for the viscous stress $\mathbf{t}_\eta = \mathbf{n} \cdot \mathbf{T} = \mathbf{n} \cdot (2\,\eta\,\dot{\boldsymbol{\varepsilon}})$ and the other for the hydrodynamic pressure $\mathbf{t}_\mathrm{p} = \mathbf{n} \cdot (-p\,\mathbf{I})$, the sum being of course the total traction $\mathbf{t} = \mathbf{t}_\eta + \mathbf{t}_\mathrm{p}$. The term $\mathbf{n}$ is the unit normal vector pointing outward from the solid boundary of the impeller system (i.e. pointing into the fluid). After obtaining the viscous traction vector $\mathbf{t}_\eta$, the torque by viscous stress can be calculated with[1]

$$\mathbf{T}_\eta = \int_\mathrm{imp} \mathbf{r} \times \mathbf{t}_\eta \, dA \tag{4}$$

The integration is over the impeller system, namely the shaft and the four vane blades connected to it. The term $\mathbf{r}$ is the vector location of the solid boundary of the impeller system and the integrand dA is in terms of surface area. The torque in the axis of the shaft is calculated by $T_\eta = \mathbf{T}_\eta \cdot \mathbf{i}_z$, in which $\mathbf{i}_z$ is the unit vector in the axis of the shaft (i.e. here the z–axis).

In the same manner as above, the torque by hydrodynamic pressure is calculated with[1]

$$\mathbf{T}_\mathrm{p} = \int_\mathrm{imp} \mathbf{r} \times \mathbf{t}_\mathrm{p} \, dA \tag{5}$$

The torque in the axis of the shaft is $T_\mathrm{p} = \mathbf{T}_\mathrm{p} \cdot \mathbf{i}_z$ and the computed total shaft torque is then $T = T_\eta + T_\mathrm{p}$. The computed total shaft torque T is the same as the measured torque[1]. Here, the total shaft torque T will also be designated as *total torque* for simplicity. For the same reason, the shaft torque by hydrodynamic pressure T_p will be designated as *pressure–torque* and the shaft torque by viscous stress T_η as *viscous–torque*.

RESULTS

The aim of the current work is to calculate the shaft torque at different angular velocities ω and compare the effect of hydrodynamic pressure p to the effect of apparent viscosity η. With this specific objective, one should keep in mind that there is a direct relationship between the apparent viscosity η and the viscous–torque $T_\eta = \mathbf{T}_\eta \cdot \mathbf{i}_z$ by $\mathbf{r} \times \mathbf{t}_\eta = \eta\,[2\,\mathbf{r} \times (\mathbf{n} \cdot \dot{\boldsymbol{\varepsilon}})]$ in Eq. (4). There is also a direct relationship between the hydrodynamic pressure p and the pressure–torque $T_\mathrm{p} = \mathbf{T}_\mathrm{p} \cdot \mathbf{i}_z$ by $\mathbf{r} \times \mathbf{t}_\mathrm{p} = -p\,[\mathbf{r} \times (\mathbf{n} \cdot \mathbf{I})] = p\,(\mathbf{n} \times \mathbf{r})$, used in Eq. (5).

Case 1: $k = 10\ \mathrm{Pa \cdot s^n}$

Fig. 2 shows the computed shaft torque as a function of angular velocity ω when the consistency index is $k = 10\ \mathrm{Pa \cdot s^n}$, yield stress is $\tau_0 = 0.1$ Pa, power-law exponent is $n = 0.5$ and density is $\rho = 990\,\mathrm{kg/m^3}$. Two torque values are shown in this figure. One is the total torque $T = T_\eta + T_\mathrm{p}$, while the other torque value is the viscous–torque T_η. The difference between the total torque T and the viscous–torque T_η is of course the contribution by hydrodynamic pressure T_p. This is clearly indicated in the figure.

From Fig. 2, it is clear that the majority

of the total torque T originates from the effect of hydrodynamic pressure p, reflected in relatively high T_p. That is, the effect of hydrodynamic pressure constitutes more than 80% of the overall torque T registered by the rheometer. This highlights the importance of understanding what influence the hydrodynamic pressure p during a measurement.

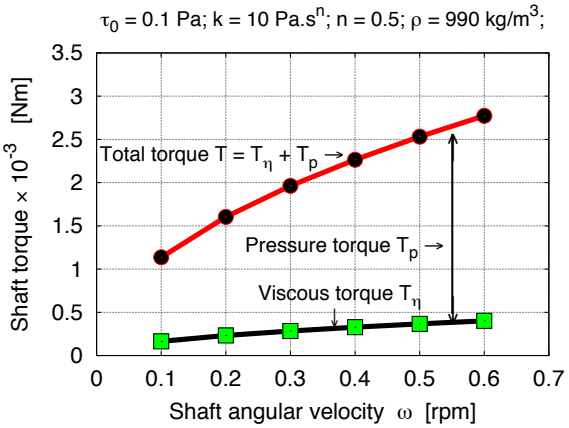

Figure 2. Shaft torque values T_η and $T = T_\eta + T_\mathrm{p}$ as a function of ω.

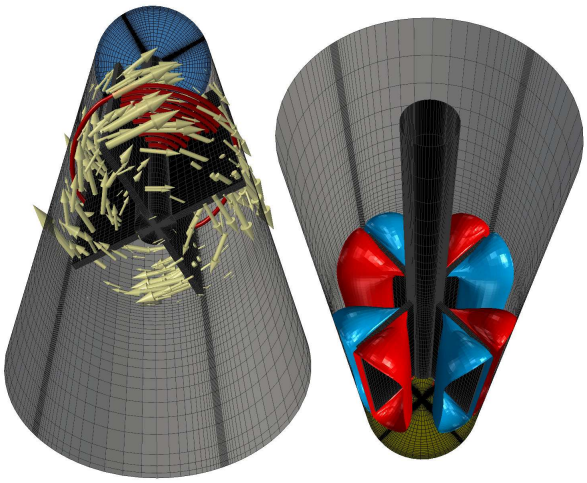

Figure 3. An example of a simulation result for the case shown in Fig. 2.

As an example of a single simulation result from the case of Fig. 2, then in Fig. 3 is a result that applies at $\omega = 0.5\,\mathrm{rps}$. The left illustration demonstrates velocity vectors $\mathbf{U}$, including streamlines at the height $z = 50\,\mathrm{mm}$ (relative to the bottom of the cylinder). The right illustration shows iso-plots of the hydrodynamic pressure. For this last–mentioned illustration, the red surface represents 20 Pa gage, while the blue surface represents −20 Pa gage. In this work, the hydrodynamic pressure is calculated in terms of gage pressure (also gauge pressure) and not in terms of absolute pressure.

Case 2: $k = 1\ \mathrm{Pa \cdot s}^n$

Fig. 4 shows the same type of result as for Fig. 2, in which now the consistency index is $k = 1\ \mathrm{Pa \cdot s}^n$. Other material parameters are the same as in Fig. 2 (i.e. Case 1). Compared to the previous case (Fig. 2), the effect of the hydrodynamic pressure p (represented with T_p) is about the same, relatively speaking. That is, the effect of hydrodynamic pressure constitutes more than 80% of the overall torque T registered by the rheometer.

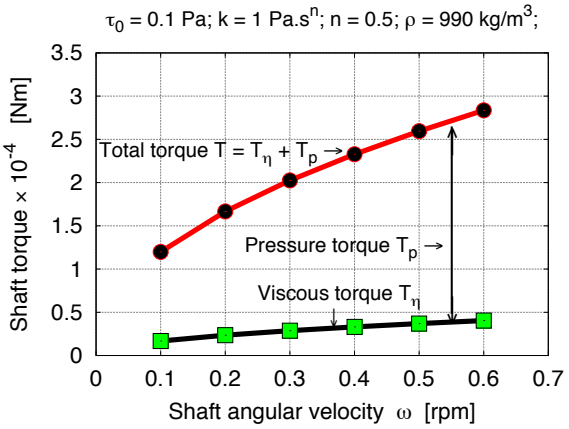

Figure 4. Shaft torque values T_η and $T = T_\eta + T_\mathrm{p}$ as a function of ω.

Case 3: $k = 0.1\ \mathrm{Pa \cdot s}^n$

Fig. 5 shows the same type of result as for Figs. 2 and 4, in which now the consistency index is $k = 0.1\ \mathrm{Pa \cdot s}^n$. Other material parameters are the same as in Figs. 2 and 4. Compared to the previous cases, the effect of the hydrodynamic pressure p (represented with T_p) is now even higher in generating the total torque T. That is, the effect of hydrodynamic pressure now constitutes close to 90% of the torque T registered by the rheometer. The

reason for this increased effect of hydrodynamic pressure p for such low viscous case (i.e. $k = 0.1\ \mathrm{Pa} \cdot \mathrm{s}^n$) is well explained elsewhere[1].

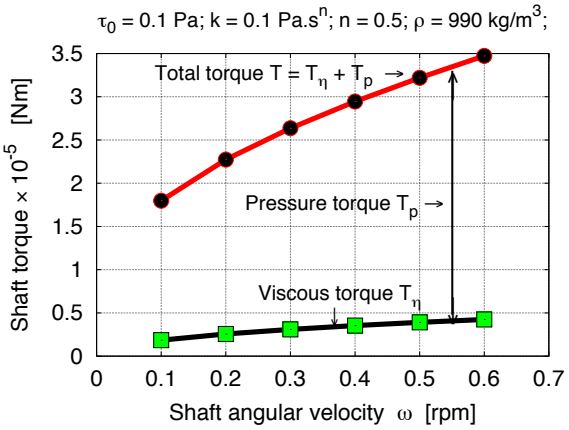

Figure 5. Shaft torque values T_η and $T = T_\eta + T_\mathrm{p}$ as a function of ω.

CONCLUSIONS

The majority of the total torque T from the vane rheometer originates from the effect of hydrodynamic pressure p and not directly from the apparent viscosity η.

As the apparent viscosity η decreases (here, by the reduction in consistency index k), the effect of hydrodynamic pressure p increases. A physical explanation of this peculiar behavior is available elsewhere[1].

ACKNOWLEDGEMENTS

This work has been funded by The Icelandic Centre for Research (RANNIS) – Grant Number 110028021 – *Computational Material Modeling.*

REFERENCES

1. Wallevik, J.E. (2014), "Effect of the hydrodynamic pressure on shaft torque for a 4-blades vane rheometer", *Int. J. Heat Fluid Flow*, http://dx.doi.org/10.1016/j.ijheatfluidflow.2014.06.001.

2. Nazari B., Moghaddam R.H., and Bousfield D. (2013), "A three dimensional model of a vane rheometer", *Int. J. Heat Fluid Flow*, **42**, 289 – 295.

3. Weller H.G., Tabor G., Jasak H., and Fureby C. (1998), "A tensorial approach to computational continuum mechanics using object-oriented techniques", *Comput. Phys.*, **12**, 620 – 631.

4. Berberović E. (2010), "Investigation of Free-surface Flow Associated with Drop Impact: Numerical Simulations and Theoretical Modeling" (Ph.D. thesis), Technische Universitat Darmstadt, Germany.

5. ANSYS FLUENT 6.3 User's Guide (2006), ANSYS Inc., USA.

6. Versteeg H.K., and Malalasekera W. (2007), "An Introduction to Computational Fluid Dynamics – the Finite Volume Method" (2nd ed.), Pearson Education Limited, England.

7. Karrholm F.P. (2006), "Rhie-Chow Interpolation in OpenFOAM", Department of Applied Mechanics, Chalmers Univesity of Technology, Sweden.

8. Tanner, R.I. and Walters, K. (1998), "Rheology: An Historical Perspective", Elsevier Science, Netherlands.

9. Barnes H.A., Hutton J.F., and Walters K. (1989), "An Introduction to Rheology", Elsevier Science, Netherlands.

10. Malvern, L.E. (1969), "Introduction to the Mechanics of Continuous Medium", Prentice-Hall Inc., USA.

11. Mase, G.E. (1970), "Schaums Outline Series: Theory and Problems of Continuum Mechanics", McGraw-Hill Inc., USA.

12. Oldroyd, J.G. (1947), "A Rational Formulation of the Equations of Plastic Flow for a Bingham Solid", *Proc. Camb. Philos. Soc.*, **43**, 100 – 105.